Visualization of the three-dimensional structure of the human centromere in mitotic chromosomes by superresolution microscopy

Elena Di Tommaso[a], Valeria de Turris[b], Pavan Choppakatla[c], Hironori Funabiki[c], and Simona Giunta[a,c,*]

[a]Laboratory of Genome Evolution, Department of Biology & Biotechnology Charles Darwin, Sapienza University of Rome, Rome 00185 Italy; [b]Center for Life Nano- & Neuro-Science, Istituto Italiano di Tecnologia (IIT), Rome 00161 Italy; [c]Laboratory of Chromosome and Cell Biology, The Rockefeller University, New York, NY 10065

ABSTRACT The human centromere comprises large arrays of repetitive α-satellite DNA at the primary constriction of mitotic chromosomes. In addition, centromeres are epigenetically specified by the centromere-specific histone H3 variant CENP-A that supports kinetochore assembly to enable chromosome segregation. Because CENP-A is bound to only a fraction of the α-satellite elements within the megabase-sized centromere DNA, correlating the three-dimensional (3D) organization of α-satellite DNA and CENP-A remains elusive. To visualize centromere organization within a single chromatid, we used a combination of the centromere chromosome orientation fluorescence in situ hybridization (Cen-CO-FISH) technique together with structured illumination microscopy. Cen-CO-FISH allows the differential labeling of the sister chromatids without the denaturation step used in conventional FISH that may affect DNA structure. Our data indicate that α-satellite DNA is arranged in a ring-like organization within prometaphase chromosomes, in the presence or absence of spindle's microtubules. Using expansion microscopy, we found that CENP-A organization within mitotic chromosomes follows a rounded pattern similar to that of α-satellite DNA, often visible as a ring thicker at the outer surface oriented toward the kinetochore–microtubule interface. Collectively, our data provide a 3D reconstruction of α-satellite DNA along with CENP-A clusters that outlines the overall architecture of the mitotic centromere.

INTRODUCTION

Chromatin folding has recently been probed in detail through the use of Hi-C techniques (Gibcus, Samejima, Goloborodko, *et al.*, 2018) and multiplexed superresolution fluorescence in situ hybridization (FISH) imaging (Bintu, Mateo, *et al.*, 2018; Su, Zheng, Kinrot, Bintu, *et al.*, 2020), yet the presence of repetitive DNA has made it difficult to analyze the spatial organization of the centromere. Within the human centromeres, the head-to-tail tandem monomers of α-satellite DNA are organized into higher-order repeat (HOR) units reiterated to span from 0.3 up to 5 Mb in size, depending on the chromosome (Altemose, Logsdon, Bzikadze, Sidhwani, Langley, Caldas, *et al.*, 2022a). Over the past two decades, several models have been suggested for the folding of the centromere chromatin to position the centromere-specific histone H3 variant CENP-A on the external surface of the primary constriction of condensed chromosomes (Blower, Sullivan, *et al.*, 2002; Ribeiro *et al.*, 2010; Schalch and Steiner, 2017). Such models are based on the assumption that

CENP-A placement works to facilitate the building of the kineto-chore in a location where it can make contact with the spindle micro-tubules and withstand the tension generated during the segrega-tion of sister chromatids to opposite poles (Vagnarelli and Earnshaw, 2001; Vagnarelli *et al.*, 2008; McIntosh *et al.*, 2002; Guenatri *et al.*, 2004). It is noteworthy that CENP-A nucleosomes make up only a fraction of the core centromere chromatin (Blower, Sullivan, *et al.*, 2002; Sullivan, 2010; Altemose, Logsdon, Bzikadze, Sidhwani, Lang-ley, Caldas, *et al.*, 2022a; Altemose, Maslan, Smith, Sundararajan, *et al.*, 2022b; Gershman *et al.*, 2022) and are interspersed with H3-containing nucleosomes (Bodor *et al.*, 2014). This is also evident from work using three-dimensional (3D) deconvolution microscopy of stretched chromatin fibers that revealed alternating blocks of CENP-A– and H3-containing nucleosomes in *Drosophila*, chickens, and humans (Blower, Sullivan, *et al.*, 2002; Ribeiro *et al.*, 2010; Sullivan, 2010). Evidence using electron microscopy showed that CENP-A–containing core centromere localizes at the surface of the primary constriction to link kinetochores to microtubules during mi-tosis (Marshall, Chueh, *et al.*, 2008). Previous work using structured illumination microscopy (SIM) and stochastic optical reconstruction microscopy (STORM) in *Xenopus* egg extracts and tissue culture cells showed that both the outer and inner kinetochore regions are transiently organized in a ring shape (Wynne and Funabiki, 2016). Recently, the dimerization of CENP-B proteins was found to contrib-ute to structural integrity upon microtubule pulling during mitosis (Chardon, Japaridze, *et al.*, 2022). However, how the DNA itself is organized so that CENP-A nucleosomes are clustered at the lateral surface of the primary constriction remains unclear. Several chroma-tin folding models have been suggested: 1) the solenoid/repeat-subunit model, where chromatin is coiled from the *p* arm to the *q* arm across the primary constriction with CENP-A–containing nu-cleosomes interspersed with H3-containing nucleosomes and ex-posed toward the kinetochore (Zinkowski *et al.*, 1991; Blower, Sullivan, *et al.*, 2002; Sullivan and Karpen, 2004; Birchler *et al.*, 2009); 2) the looping model, where centromeric chromatin is looped out from bulk chromatin toward the spindle pole (Dalal *et al.*, 2007; Yeh, Haase, *et al.*, 2008); and 3) the layered boustrophedon (Ribeiro *et al.*, 2010), where sinusoids are layered so that CENP-A– and H3-containing nucleosomes are exposed on the surface of the centro-meric chromatin to interact with kinetochore proteins. Additional complexity is given by the fact that the centromeric chromatin is likely to be coiled, folded, or looped several times to form a multi-layered structure (Marshall, Chueh, *et al.*, 2008).

In 2017, Schalch and Steiner noted that, "imaging higher order chromatin to derive folding patterns seems currently beyond the limit of microscopy" (Schalch and Steiner, 2017), yet recent advances in superresolution through SIM, expansion microscopy (ExM), and several other technologies offer new opportunities to probe the organization of DNA within mitotic chromosomes. The recent assembly of human centromere sequences in the CHM13 reference genome derived from a molar pregnancy (Nurk, Koren, Rhie, Rautiainen, *et al.*, 2022) established that the active centromeres of most human chromosomes are composed of a dominant segment of largely unidirectionally oriented α-satellite DNA repeats (Altemose, Logsdon, Bzikadze, Sidhwani, Langley, Caldas, *et al.*, 2022a). Consis-tent with this tandem organization of the α-satellite repeats, the use of chromosome orientation FISH (CO-FISH) allows the hybridization of centromere-specific probes uniquely to the one strand of the α-satellite in a single chromatid (Giunta, 2018). This technique has pro-vided specific and quantitative staining of each centromere in the two sister chromatids within the primary constriction of mitotic chro-mosome. It also can identify sister chromatid exchanges indicative of

recombination events within centromeric DNA that we have shown to be exacerbated upon depletion of CENP-A during presenes-cence and in cancer cell lines (Giunta and Funabiki, 2017). To further examine the distribution of the α-satellite repeats at the primary con-striction, here we combined centromere CO-FISH (Cen-CO-FISH) and 3D SIM, which visualizes centromere organization within a single chromatid while preserving DNA morphology in the absence of a high-temperature denaturation step used in conventional FISH that can impact chromatin. Our data indicate that α-satellite repeats are arranged in a ring-like configuration with a low fluorescence intensity core resembling the CENP-A rosette-like structure observed in inter-phase nuclei (Andronov, Ouararhni, *et al.*, 2019). Furthermore, using ExM, we found that CENP-A organization within mitotic chromo-somes follows that of the α-satellite DNA, with a ring-like organiza-tion thicker at the lateral side of the primary constriction. Our data reinforce the notion that α-satellite DNA is three-dimensionally orga-nized in a way to favor outer kinetochore assembly and provide new insight into the arrangement of centromeric DNA within human mi-totic chromosomes.

RESULTS

We used 3D SIM to visualize the organization of α-satellite DNA lo-calized in the core centromeric region within mitotic chromosomes in the immortalized retinal epithelial cells RPE-1 (RPE-1-h-TERT). We obtained prometaphase chromosomes by colcemid treatment of asynchronous cells for 2 h, which induced disruption of microtubules and mitotic arrest in the subset of cells entering mitosis in the given time window (Rieder and Palazzo, 1992). We hypotonically swelled chromosomes before fixation and proceeded using the Cen-CO-FISH protocol (Giunta, 2018) to differentially stain the centromeres of each sister chromatid using Alexa-488 and Cy3 fluorophores to stain them in green and red, respectively (Supplemental Figure 1A). Labeling of the centromeres by CO-FISH utilizes short, fluorescently tagged peptide nucleic acid (PNA) probes complementary to a re-petitive consensus sequence in the α-satellite array. We used a PNA probe set against a 17-base-pair conserved feature in the α-satellite monomer, the CENP-B box (Supplemental Figure 1B, CENP-B Box probe set 1). First, we performed 3D SIM using the DeltaVision OMX platform to image Cen-CO-FISH–stained prometaphase chromo-somes, which allowed us to resolve the centromere green and red "blobs" obtained by conventional deconvolution microscopy with a higher level of detail (Figure 1A). 3D SIM analysis of centromere DNA showed a heterogeneous pattern (Figure 1A), with several chromosomes displaying a distinctive organization with a low-inten-sity region in the middle of the volumetric surface located at the primary constriction (Figure 1B, Supplemental Video 1, and Supple-mental Figure 2B). This ring-like structure appears more visible on the Alexa-488–labeled probe, which gave the best resolution due to its tighter emission and excitation, compared with the longer-emis-sion wavelength of the Cy3 fluorophore (Schermelleh *et al.*, 2010). Yet, even with the red probe, we found several examples of ring-like centromere DNA organization with a dip in fluorescence intensity localized in the center of the 3D surface (Supplemental Figure 1D).

To confirm the presence of a region of reduced signal intensity in the center of the centromere configuration (Figure 2A), we per-formed a line scan analysis of the fluorescence intensity across the Alexa-488 surface for all centromeres imaged in our study. Both ver-tical and horizontal lines across the centromere gave two peaks of fluorescence around a central dip in signal often nearing back-ground levels (Figure 2B). Next, we verified whether the centromeric chromatin corresponding to the middle of the centromere rings was stained with 4,6-diamidino-2-phenylindole (DAPI) or completely
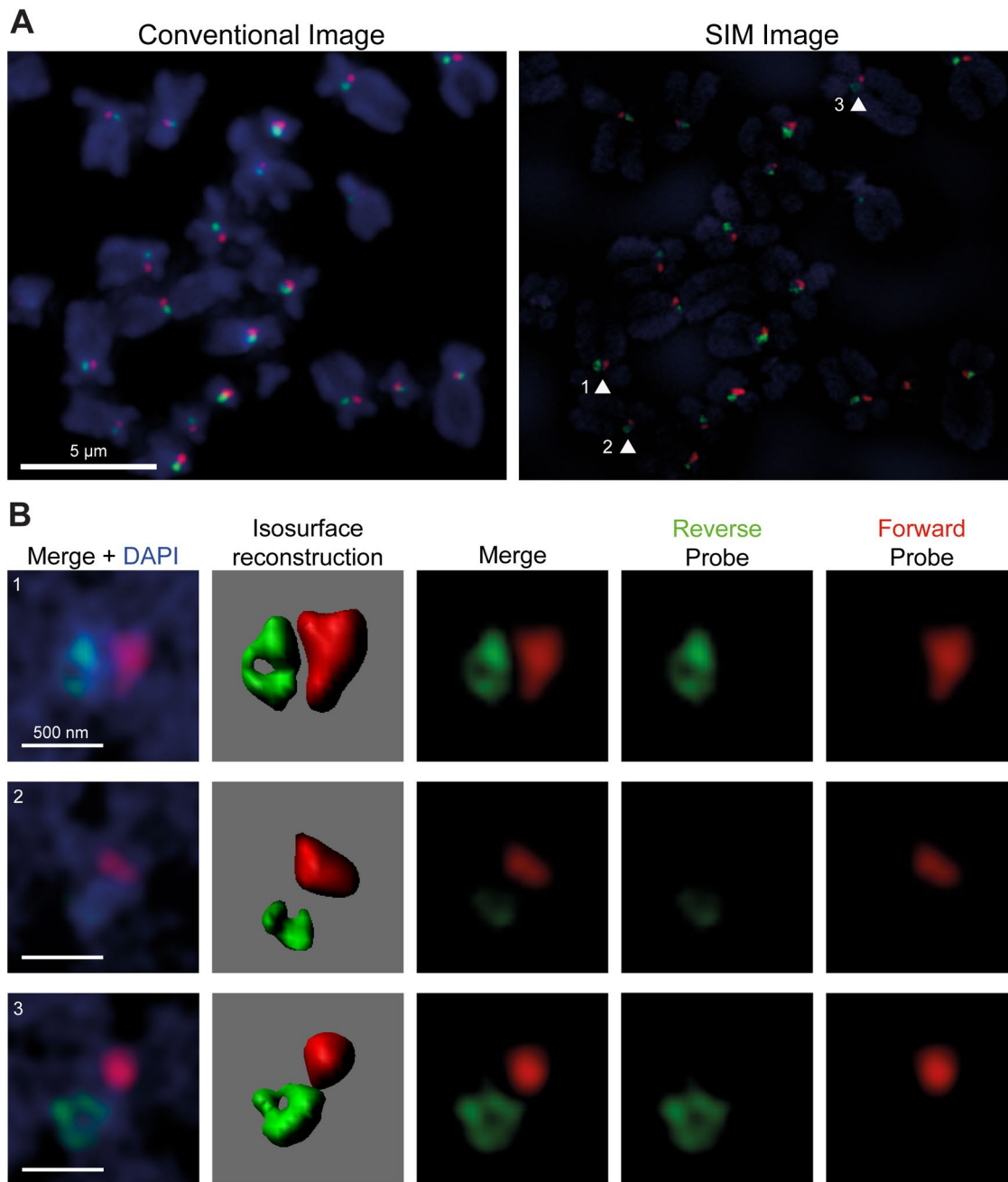
FIGURE 1: 3D SIM of centromere DNA stained by Cen-CO-FISH in human mitotic chromosomes using OMX Delta Vision. (A) Conventional deconvolution microscopy (left panel) and SI (right panel) maximum-projection images of the same prometaphase chromosomes of human RPE-1-hTERT as stained by Cen-CO-FISH (CENP-B box probe set 1); scale bar is 5 μm. White arrows indicate chromosomes with a ring-like staining pattern of centromere DNA. (B) Examples of max projection and isosurface reconstruction of ring-like arrangements indicated by the white arrows and numbered in the metaphase spread in A; scale bar is 500 nm.

depleted of fluorescence. We found that 95% of all centromeres display DAPI-positive staining in the center of the ring (Supplemental Figure 1F), with the remaining 5% of chromosomes presenting a depletion of signal from all the fluorophores at the center of the ring (Supplemental Figure 1G). These data imply that, in most centromeres, ring-forming α-satellite HORs are wrapped or overlaid around noncentromeric DNA, likely made up of divergent α-satellite monomers and flanking pericentromere (see *Discussion*).

To validate the pattern obtained with the CENP-B Box Probe Set 1, we performed Cen-CO-FISH using another set of probes (Giunta and Funabiki, 2017) that hybridizes against a different 18-base-pair consensus sequence conserved within the α-satellite monomer (Figure 2E; Supplemental Figure 1B, α-satellite probe). This gave rise to a hybridization pattern (Figure 2E and Supplemental Figure 2A) similar to the one obtained with CENP-B box probe set 1 (Supplemental Figure 2B), suggesting that the details visualized by 3D SIM reflect the *bona fide* structured distribution of centromere α-satellite DNA within the human prometaphase chromosomes. To calculate the percentage of ring-like centromeres on the total number of chromosomes for each metaphase spreads imaged
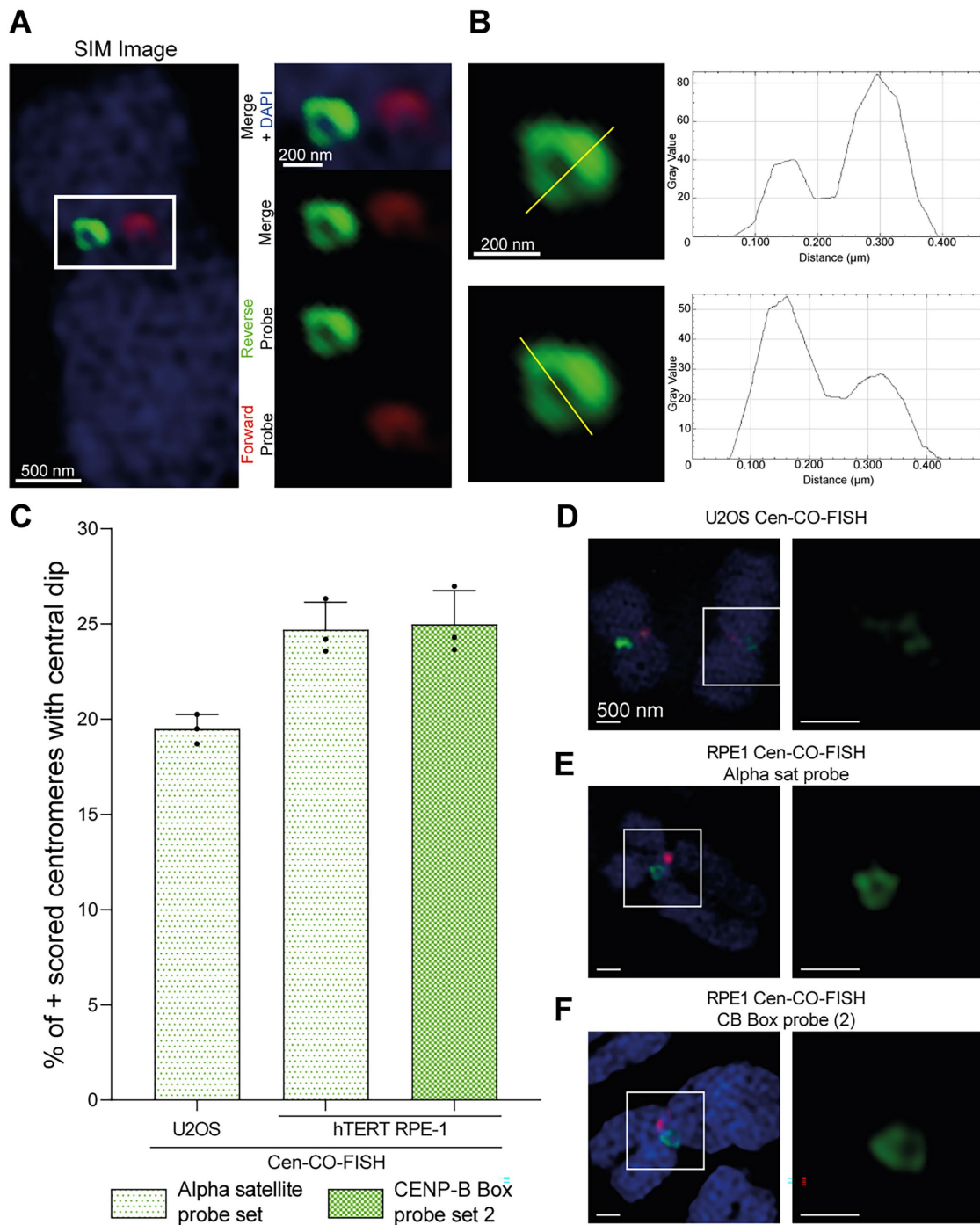
FIGURE 2: Metaphase ring-like organization of human centromeric DNA is preserved under different conditions. (A) Maximum projection of human mitotic chromosome stained by Cen-CO-FISH with CENP-B box probe set 1; scale bar is 500 nm. White box area is enlarged on the right-hand side. Individual channels with green probe, red probe, and merged images (with and without DAPI) are shown. (B) Line scan analysis of green probe of centromere as in A. (C) Percentages of positive scored Alexa-488–labeled centromeres forming a ring over the total number of centromeres. For each individual experiment, 200–700 chromosomes were counted. The error bars show the SD of the mean across three biological replicates. (D–F) Example of one chromosome for each condition as plotted in C with a zoom-in on the green probe; scale bar in each square is 500 nm. (D) U2OS chromosome stained by Cen-CO-FISH with α-satellite probe. (E) RPE-1 chromosome stained by Cen-CO-FISH with α-satellite probe. (F) Example of RPE-1 chromosome stained by Cen-CO-FISH with CENP-B box probe (set 2).

throughout this study, we used the pipeline shown in Supplemental Figure 1C and counted the centromeres presenting a two-peak line scan graph as shown in the examples in Supplemental Figure 1D. In our quantifications, we excluded line scan graphs where one of the two peaks did not show fluorescence intensity higher than the central dip (Supplemental Figure 1E). About 25% of the centromeres within each metaphase spread presented a line scan graph with two peaks of fluorescence around a central dip of lower fluorescence

intensity representing the ring-like structure (Supplemental Figure 1D). Furthermore, we observed ring-like patterns whether we used the CENP-B box set 1 or the α-satellite probe (Supplemental Figure 2, B and A, respectively; also quantified quantified in Figure 2C) to similar percentages independently of whether the forward or the reverse probe was used first during the hybridization step. The 25% occurrence observed is consistent with the idea that the central channel of the α-satellite DNA ring can be visualized only on chromosomes with specific axial orientations relative to the Z-axis but may also be influenced by chromosome-specific DNA repeat arrangements among different centromeres. However, we favor the former interpretation as we detected the tilted ring centromere visible only in Z when a chromosome was twisted or folded (unpublished data) and found ring-like centromeres to be present across chromosome subgroups (Supplemental Figure 2, A and B).

Next, we reasoned that the Cen-CO-FISH technique (Giunta, 2018) may provide distinct advantages for superresolution imaging of chromosomal loci. CO-FISH enables the individual and differential labeling of each sister chromatid and, importantly, does not require heat for DNA denaturation. While high-temperature treatment has long been thought to disrupt chromosome morphology (Winkler et al., 2003), data are still inconclusive as to whether exposing chromosomes to temperatures above 70°C to physically separate the DNA in standard FISH protocols affects nuclear structures (Markaki et al., 2013). Using CO-FISH, the anneal of strand-specific probes is obtained by exposing the DNA through enzymatically digesting the newly synthesized strand (Supplemental Figure 1A). We performed conventional FISH using the Alexa-488–labeled α-satellite probe to assess whether we could visualize the rings following a standard heat denaturation step. While we still retained some ring-like structures, they were found in only 12% of chromosomes (Supplementary Figure 2D) with a more diffused staining and less visible patterning (Supplemental Figure 2D) across all chromosomes, suggesting that the chromatin conformation was affected by the high-temperature treatment. The fact that we still observed the ring-like patterned organization in some chromosomes after the denaturing step suggests that the centromere rings are unlikely to result from the irregular accessibility of the probes.

To verify that this patterned organization is not exclusive to centromere DNA in RPE-1 cells, we used U2OS cells derived from human osteosarcoma. We performed Cen-CO-FISH using the α-satellite probe and imaging by 3D SIM. We found a configuration of the α-satellite DNA distribution similar to the ring-like pattern in RPE-1 (Figure 2D and Supplemental Figure 2C) to approximately 20% (Figure 2C), implying that centromere rings are present in human cell lines from different tissues. The overall change in centromeric chromatin in cancer cells (Sullivan, Boivin, et al., 2011; Giunta and Funabiki, 2017) and our previously reported increase in centromere DNA recombination (Giunta and Funabiki, 2017) may account for the slight decrease in the percentage of ring-like centromere structures, as well as the possible variation in the repeats sequence, size, and order affecting their chromatin organization. In line with our previous data using superresolution microscopy and Cen-CO-FISH showing changes in the volume of the centromere DNA upon CENP-A depletion (Giunta and Funabiki, 2017), we concluded that distribution, size, and shape of the centromere α-satellite DNA can show variation between chromosomes and under different cellular conditions while retaining a visible ring-like organization.

We further validated the presence of the centromere ring-like DNA pattern through 3D SIM using a different imaging platform, the Zeiss Elyra 7 (Figures 2F and 3A, Supplemental Figures 2E and 3A, and Supplemental Video 2). As for the OMX, we analyzed human

metaphase spreads obtained by colcemid treatment of RPE-1-hTERT cells stained using CENP-B box probes (Supplemental Figure 1B, CENP-B box probe set 2). We applied the line scan method (Supplemental Figure 1, C–E) to quantify all metaphase spreads imaged across three independent experiments and found a frequency of ring-like centromeres similar to the one observed with the OMX platform of ~25% (Figure 2C) with the same size and configurations (Figure 3A and Supplemental Figure 2E). Again, we observed that the green probe showed better resolution compared with the red one regardless of the probe sequences, CENP-B box (sets 1 and 2) and the α-satellite probe set, or the SIM imaging platform (Supplemental Figures 1B and Figure 2C). Yet ring configurations can be rendered by isosurfaces (Figure 3A, Supplemental Figure 3A, and Supplemental Video 4), Z-scan (Figure 3B), and line scan analysis for both Alexa-488– and Cy3-labeled probes (Figure 3, C and D, respectively). We also measured area (Supplemental Figure 3B), volume (Supplemental Figure 3C), intensity mean (Supplemental Figure 3D), and intensity sum (Supplemental Figure 3E) of both Alexa-488– and Cy3-labeled chromatids of every centromere from 20 metaphase spreads of human RPE-1-hTERT stained by Cen-CO-FISH. In each one of the metaphase spreads analyzed, we obtained similar distributions of the area and volume of the different centromeres in the same cell (Supplemental Figure 3, B and C) going from an area of 0.3 μm^2 to 1.6 μm^2, proportionally compatible with the amount of α-satellite DNA present in each chromosome, known to span from 0.3 to 5 Mb in size (Altemose, Logsdon, Bzikadze, Sidhwani, Langley, Caldas, et al., 2022a).

From our data, whether the ring-like organization is specific to centromeres of colcemid-arrested prometaphase chromosomes due to the absence of microtubules or whether it is retained under tension is unclear. To address this, we performed Cen-CO-FISH staining of asynchronous mitotic cells in the absence of colcemid or any other microtubules' poisons. As expected, without colcemid we obtained a lower number of mitotic cells and a closer proximity of the chromosomes to each other (Supplemental Figure 4B) compared with in colcemid-treated prometaphases (Supplemental Figure 4A). Even in the absence of microtubule depolymerizing agents, we were still able to see 22% ring-like centromeric patterns (Supplemental Figure 2F). We also observed ring-like configurations of centromere DNA in an example of an anaphase cell where we could identify segregated sister chromatids thanks to the visible separation of Cen-CO-FISH probes (Supplemental Figure 4C), indicating not only that the ring-like organization is present under conditions of microtubule depolymerization and after mitotic arrest, but also that the structural organization of human chromosomes at the centromere may be preserved beyond metaphase, throughout mitotic progression and exit.

Centromeres are enriched in both α-satellite DNA and CENP-A chromatin. Though CENP-A nucleosomes constitute a small fraction of all nucleosomes at the centromere (Bodor et al., 2014) and the size of α-satellite regions loaded with CENP-A varies between chromosomes, the total amount of CENP-A is correlated with each variant of α-satellites in a number of cell types (Sullivan, Boivin, et al., 2011). Our SIM imaging of α-satellite DNA shows an arrangement of centromeric DNA that might serve to position CENP-A–rich chromatin at the region proximal to the kinetochore. To check the distribution of CENP-A protein, we employed ExM. Colcemid-arrested RPE-1-hTERT cells were fixed with 2% paraformaldehyde (PFA), stained with CENP-A antibodies and the corresponding secondary, and expanded using the protocol reported by Chozinski and colleagues (Figure 4A) (Chozinski, Halpern, et al., 2016). ExM results show that CENP-A may not be distributed uniformly as one would expect for a "plate-like" monolayer
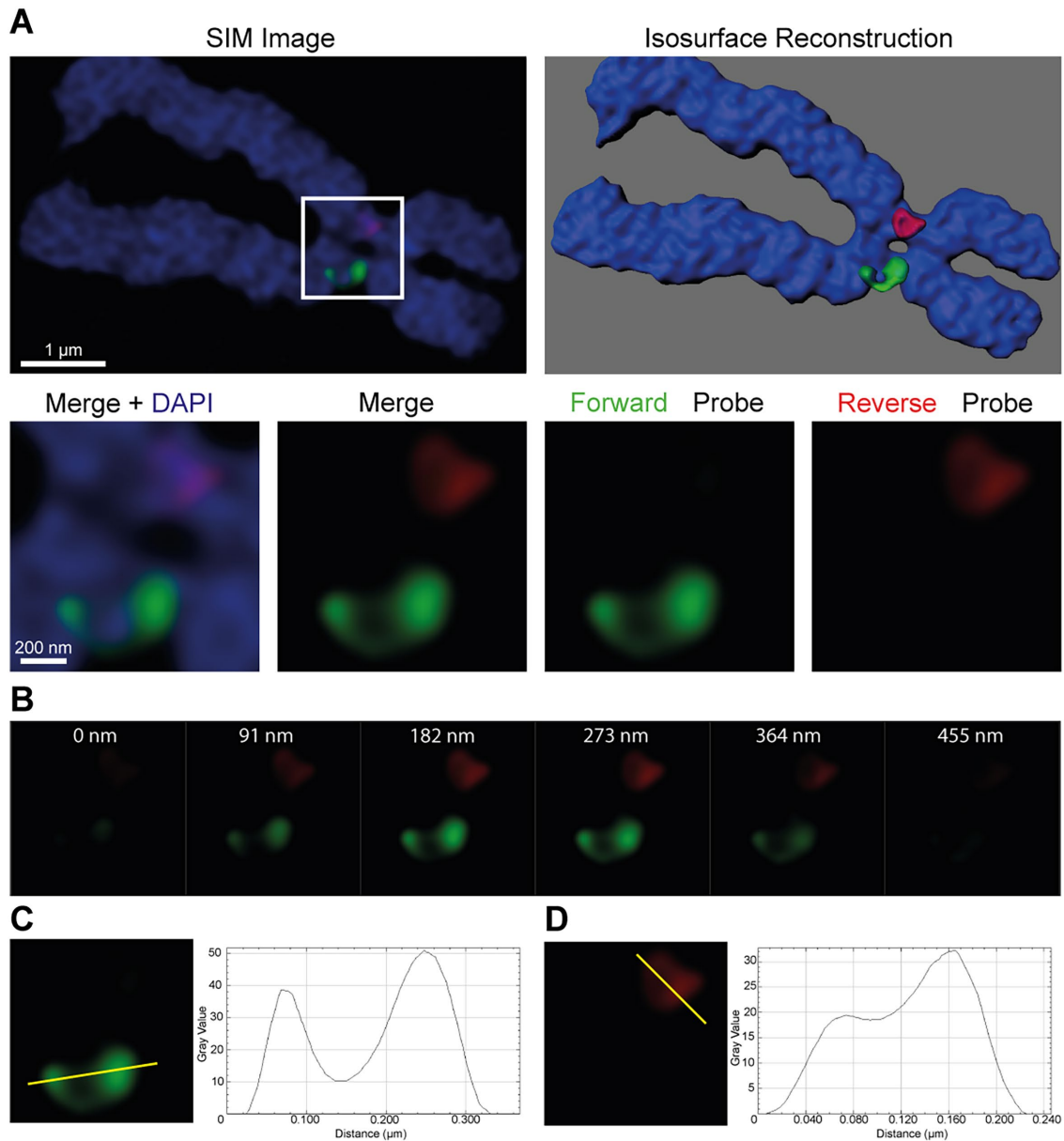
FIGURE 3: 3D SIM of centromere DNA stained by Cen-CO-FISH in human mitotic chromosomes using Zeiss Elyra 7 also shows ring-like structures. (A) SIM maximum-projection and isosurface reconstruction images of the same chromosome of human RPE-1-hTERT cells stained by Cen-CO-FISH; scale bar is 1 μm. White box area is enlarged below the individual channels, the merge, and the merge with the DAPI; scale bar is 200 nm. (B) Z-scan analysis of the centromere as in A. (C, D) Line scan analysis of Alexa-488 and Cy3 probe, respectively, of the centromere as in A.

configuration (Cleveland *et al.*, 2003; Santaguida and Musacchio, 2009) but may form several distinct clusters that jointly assemble into a ring-like configuration for a subset of chromosomes (Figure 4B). The diameter of the expanded CENP-A patterned distribution is around 600–800 nm (Figure 4B). Using the chromosome width as a marker, we can obtain a rough estimate of the sample expansion of around 4.5-fold. This gives an estimated real ring size of around 150–200 nm, which is similar to values observed with Cen-CO-FISH for α-satellite arrays. Notably, we observed enrichment of CENP-A signals at the lateral side of the primary constriction with a substantial gap between the sister pairs (Figure 4C), implying that the CENP-A ring is often thicker on the outer interface oriented toward the spindle's microtubules, forming a heterogeneous crescent-like staining of CENP-A (Figure 4B) rather than a full ring as we ob-

served for the α-satellite DNA (Figure 2A). This type of organization suggests that the centromere ring may serve for the lateral positioning of the CENP-A–rich chromatin to favor the kinetochore assembly. In addition, other extended structures can be seen in the expanded CENP-A images (Figure 4C) that were also observed in the patterns of α-satellite DNA obtained by 3D SIM (Figure 1A). It is unclear whether these additional types of patterned organization resemble variation in DNA, chromatin, chromosomes, or kinetochore structures (Magidson, Paul, *et al.*, 2015) or a higher variation in the orientation of the centromeres during sample preparation. Altogether, our data present evidence of ring-like organization of centromere DNA and chromatin at superresolution that can help improve our understanding of the 3D centromere organization in human mitosis.
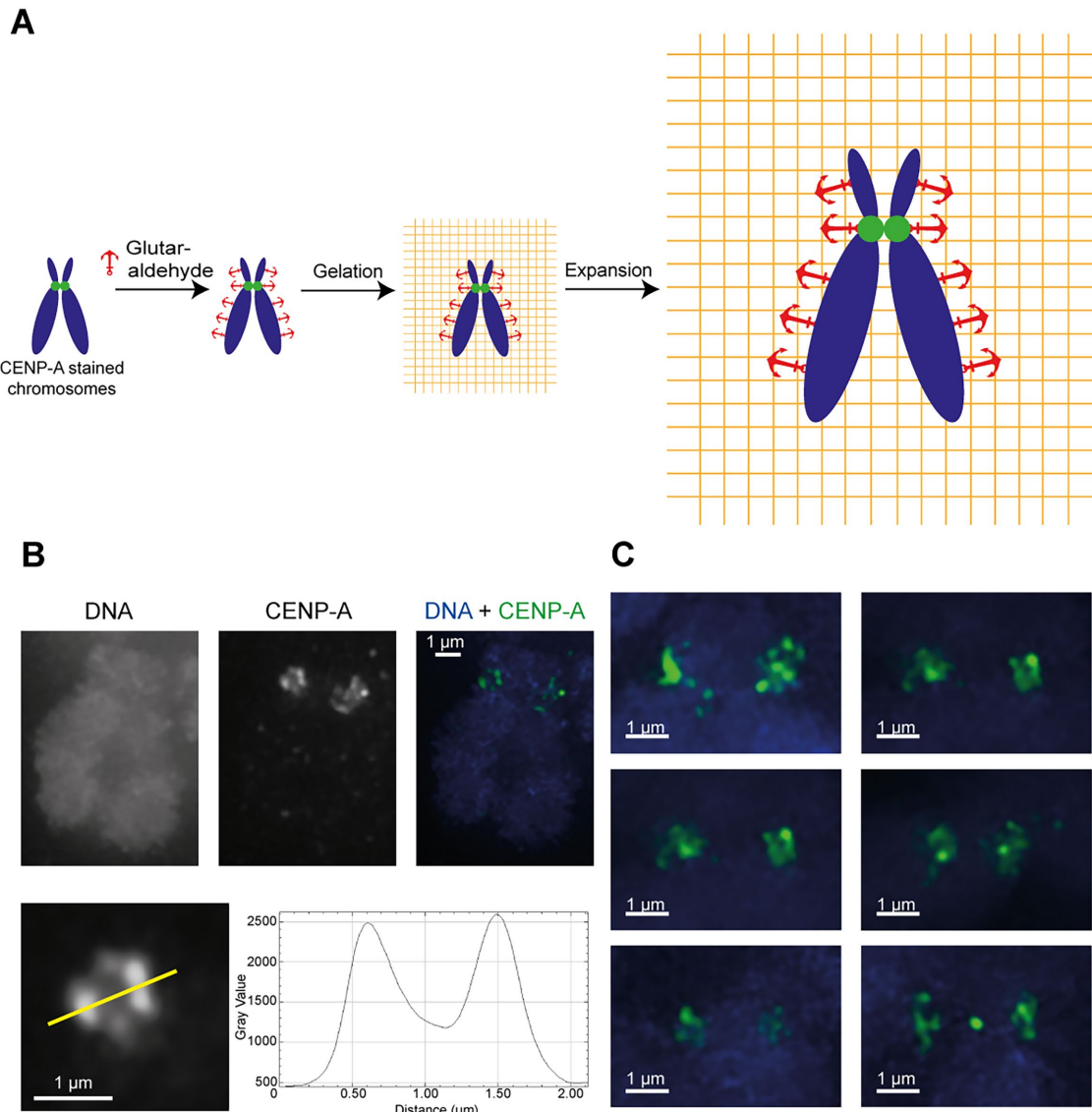
FIGURE 4: ExM on CENP-A–stained RPE-1-hTERT mitotic cells shows similarity between the structural organization of centromere chromatin and DNA. (A) Protocol for ExM of RPE-1 cells showing cross-linking, gelation, and expansion steps. Blue, DNA; green, antibody-labeled CENP-A. Orange grid represents acrylamide gel. (B) Metaphase chromosome showing ring-like structure (top), zoomed region (yellow box) shown below right, and line scan of the indicated (yellow line) CENP-A signal (below right); scale bar is 1 µm. (C) Additional examples of ring-like CENP-A loci. Color scheme same as in B.

DISCUSSION

Here, we used 3D SIM to visualize the organization of α-satellite DNA repeats within mitotic chromosomes. Our data indicate that centromere α-satellite DNA is arranged in a ring-like configuration with CENP-A, forming several distinct staining clusters preferentially localized on the lateral side (Figure 5A), likely oriented so that the microtubules can attach to its side to pull sister chromatids apart during mitosis. Our study also highlights the use of Cen-CO-FISH (Giunta, 2018) as a valuable technique for high-end imaging studies to visualize repetitive sequence organization within a single chromatid while preserving DNA morphology in the absence of the denaturation step required in conventional FISH. Cen-CO-FISH uses enzymatic digestion to expose the DNA, allowing hybridization of the probes in a more physiological chromatin environment that has not been perturbed by high temperatures. Our data suggest that the FISH protocol with a denaturation step at 80°C for 5 min partly alters

the DNA organization of human centromeres, whereas applying the Cen-CO-FISH technique before superresolution imaging may help to better preserve it.

Based on the latest genomic and epigenetic description of the human centromere in the CHM13 human genome assembly (Altemose, Logsdon, Bzikadze, Sidhwani, Langley, Caldas, *et al.*, 2022a; Gershman *et al.*, 2022; Nurk, Koren, Rhie, Rautiainen, *et al.*, 2022), the centromere α-satellite monomers organized into HOR arrays present high sequence identity, providing complementary loci for hybridized probes that are regularly spaced in close proximity. Because each probe is labeled by a single fluorophore, Cen-CO-FISH labeling relies on the high density of binding sites to jointly provide detectable staining of centromeric HORs (Figure 5A, higher-order repeats (HORs) array). On the other hand, the flanking regions are made up of more divergent repetitive DNA where α-satellite monomers lose their higher-order organization

A

1) Monomeric — Higher Order Repeats (HORs) Array — Monomeric
CDR

2) Centromeric chromatin

3) Alpha-satellite ring-like organization with CENP-A staining model

B Looping Model

C Repeat-subunit (Solenoid) Model

D Boustrophedon (Sinusoidal Patch) Model

E Layered Looping Model: Lateral 3D view

Layered Looping Model: Frontal view

Green labeled chromatid — Red labeled chromatid

Cartoon of Layered Looping ring-like signal

Alexa-488 labeled centromere — Cy3 labeled centromere — Centromere (A-488 labeled) — Centromere (Cy3 labeled) — Pericentromere (unlabeled)

H3 nucleosomes — CENP-A nucleosomes — CENP-A staining — Microtubules

(Altemose, Logsdon, Bzikadze, Sidhwani, Langley, Caldas, et al., 2022a); it is likely that these divergent regions where alphoid DNA is not organized in HOR have sporadic and spaced-out hybridization of our α-satellite probes, generating single-molecule fluorescence that is beyond our detection limit or no hybridization at all (Figure 5A, monomeric). In the 3D space, our observations may suggest an interesting relationship between the central HOR centromere (labeled α-satellite DNA) and the flanking pericentromere (unlabeled DNA) (Figure 5A, parts 1 and 2). In line with the previous model of layered organization, centromere and flanking pericentromere DNA may also layer each other. The centromere HOR that we detect using our Cen-CO-FISH probes may be sandwiched by DAPI signal from more divergent, unlabeled pericentromeric DNA whose fluorescence is visible at the center of the ring. While this was true for the majority of chromosomes, ~5% showed DAPI-negative staining corresponding to the middle of the ring, likely reflecting chromosome-specific differences in the centromere DNA organization or rendering issues during 3D SIM deconvolution due to DAPI diffuse signal. However, the exact nature of the DNA found in the middle of the α-satellite HOR DNA ring remains speculative and requires further investigations.

Different models have been proposed to describe centromere chromatin folding within mitotic chromosomes: 1) the looping model (Figure 5B; Dalal et al., 2007; Yeh, Haase, et al., 2008), 2) the solenoid/repeat-subunit model (Figure 5C; Zinkowski et al., 1991; Blower, Sullivan, et al., 2002; Sullivan and Karpen, 2004; Birchler et al., 2009), and 3) the sinusoidal patch/layered boustrophedon model (Figure 5D; Ribeiro et al., 2010). The looping model proposes that the centromeric chromatin is looped out from bulk chromatin toward the spindle pole (Figure 5B); in the solenoid model, the centromeric chromatin forms a coil with CENP-A–containing nucleosomes facing the spindle pole (Figure 5C); finally, the layered boustrophedon (also known as sinusoidal patch) model attempts to explain the observed location of constitutively centromere-associated network (CCAN) proteins and the unfolding of the vertebrate kinetochore (Figure 5D). These models propose an organization that favors CENP-A–containing nucleosomes to face the spindle pole to facilitate microtubule attachment. The sinusoidal patch model also allows for H3-containing nucleosomes to be present on the surface of the centromeric chromatin to interact with kinetochore proteins (Verdaasdonk and Bloom, 2011). Here, we try to reconcile the mitotic ring-like centromere structure that we observed with Cen-CO-FISH and 3D SIM with information from the previous models, taking into consideration the recent advances in understanding mitotic chromosomes folding

through chromatin loops (Gibcus, Samejima, Goloborodko, et al., 2018; Dekker and Dekker, 2022), the interposition of CENP-A-containing nucleosomes with H3-containing nucleosomes (Blower, Sullivan, et al., 2002; Sullivan and Karpen, 2004), the latest genomic data including the information that CENP-A is highly enriched in the CDR (centromeric dip region, where "dip" refers to a region with lower DNA methylation often concomitant with CENP-A chromatin enrichment; Altemose, Logsdon, Bzikadze, Sidhwani, Langley, Caldas, et al., 2022a) with respect to the rest of the active HOR array (Bodor et al., 2014; Altemose, Logsdon, Bzikadze, Sidhwani, Langley, Caldas, et al., 2022a; Gershman et al., 2022), and the concept that the mammalian kinetochore is based on the repetition of the budding yeast single structure (Yeh, Haase, et al., 2008). We propose a model where centromeric mitotic chromatin is looped in a ring structure and layered with the flanking pericentromere. In our layered looping model (Figure 5E), each layer is composed of chromatin loops similar to those in the looping model (Dalal et al., 2007; Yeh, Haase, et al., 2008) but arranged in a circular disposition that is parallel to the chromosome axis to explain the data from our Cen-CO-FISH hybridization with the α-satellite DNA resulting in the flat ring-like structure that we identified. The layered looping organization that we propose incorporates the concept of loop array formation in mitotic chromosomes mediated by condensins described in Gibcus, Samejima, Goloborodko, et al. (2018). In line with each metaphase loop containing ~250 kb, we suggest the average centromere to be made up of one to three layers, each containing ~6–10 loops of active α-satellite HOR DNA homogeneously stained by Cen-CO-FISH probes (in our model, for simplicity, we depicted only one layer), which are sandwiched between layers composed of the flanking unstained regions (Figure 5E and Supplemental Figure 5A). The loops folding and the layering of centromere and pericentromere DNA can explain the formation of the ring-like organization and the presence of DAPI staining in the central dip that we detected. While we have drawn the layers containing loops as "flower petals" to justify the central dip in signal, we cannot exclude that an alternative heterogeneous layered solenoid model may also fit our data, but only if oriented parallel to the microtubule binding interface.

As for the previously proposed models (reviewed in Verdaasdonk and Bloom, 2011; Schalch and Steiner, 2017), the outer positioning of the functional centromeric DNA containing CENP-A nucleosomes is designed to enable kinetochore attachment to microtubules for sister chromatid separation. Accordingly, our data using ExM show an enrichment of CENP-A signals at the lateral side of the primary constriction that appears to exhibit a ring-like or a crescent

FIGURE 5: Human centromere DNA and chromatin folding models in mitotic chromosomes. (A) Graphical representation of the HOR array of the centromere (labeled by Cen-CO-FISH) with CENP-A density going from approximately one every four nucleosomes in the CDR to about one every 20 in the rest of the active HOR; also shown, flanking DNA is made up of more divergent repetitive DNA including α-satellite monomers. Both are depicted as 1) linear and 2) chromatinized DNA. 3) Representation of dividing mitotic chromosomes showing ring-like centromeres observed with Cen-CO-FISH-SIM and CENP-A positioning seen with ExM. (B–D) Graphic representation of previous mitotic centromere models. (B) Looping model as described in Dalal et al. (2007) and Yeh, Haase, et al. (2008). (C) Repeat-subunit model (or solenoid model) as described (Zinkowski et al., 1991; Blower, Sullivan et al., 2002; Cleveland et al., 2003; Sullivan and Karpen, 2004; Birchler et al., 2009). (D) Boustrophedon model (also called sinusoidal patch) as described in Ribeiro et al. (2010). (E) Graphical representation of our proposed layered looping model. We suggest the mitotic centromere to be made up of loops forming a "flower-like" arrangement with CENP-A nucleosomes being positioned in a way to favor CENP-C dimerization facing the kinetochore–microtubule binding interface to enable sister chromatids segregation. The central layer made up of centromeric α-satellite HOR is sandwiched by layers of looped unlabeled DNA, possible from the flanking pericentromere. The model is shown with a 3D lateral view on the left and with a frontal view on the right for both green- and red-labeled sister chromatids. The models we show here are not to scale but are representative of previous and current models with numerically proportional representations of DNA and nucleosomes where possible.

configuration. It is tempting to speculate that this conformation serves the key functional role of placing CENP-A–rich chromatin toward the kinetochore–microtubule interface. Intriguingly, we noticed that CENP-A staining often forms several distinct clusters, implying a more modular chromatin structure than that of the previously thought homogeneous monolayer. Based on recent evidence from the Musacchio lab where two CENP-A nucleosomes together with a CENP-C dimer form a binding module sufficient to assemble a full kinetochore (Walstein *et al.*, 2021), our model depicts two CENP-A nucleosomes in the active region of the HOR on the tip of the loops interspersed with canonical nucleosomes. The exact way CENP-A is interspersed with canonical nucleosomes remains under debate, but it may be possible that CENP-A dinucleosomes flanked by canonical nucleosomes can exclusively support kinetochore assembly. Because CENP-A generally occupies between 7 and 24% of the active chromatin going from approximately one in four nucleosomes in the CDR to about one in 20 in the rest of the active HOR (Altemose, Logsdon, Bzikadze, Sidhwani, Langley, Caldas, *et al.*, 2022a; Gershman *et al.*, 2022), in our layered looping model we proportionally depicted ~10 nucleosomes positioned in a way to reflect the staining we observed by ExM, with clustered organization of CENP-A in a ring thicker at the outer centromere side.

Human prometaphase chromosomes display a ring-like centromere configuration by 3D SIM in both normal and cancer cells. We have generated models to compare the organizations of the α-satellite DNA stained using Cen-CO-FISH in immortalized RPE1 cells (Figure 5E and Supplemental Figure 5A) with the U2OS cancer cell line (Supplemental Figure 5B), as well as with RPE-1 cells stained by conventional FISH (Supplemental Figure 5C). In our previous study, we applied Cen-CO-FISH to reveal a mechanism dependent on CENP-A and its associated proteins to prevent centromere recombination in human cells, which also increases in replicative senescence and in cancer cells (Giunta and Funabiki, 2017). CENP-A contributes to centromere DNA stability (Black and Giunta, 2018) and to preventing mutagenic R-loop–induced DNA damage and chromosome rearrangements (Balzano *et al.*, 2021; Giunta, Hervé, *et al.*, 2021). We also found that CENP-A depletion causes an apparent increase in the chromatin volume occupied by α-satellites along with altered sphericity of centromeres (Giunta and Funabiki, 2017). Here, we observed a slightly lower percentage of ring-like centromere organization in the cancer cell line U2OS (Supplemental Figure 5B) that may reflect a destabilization of the chromatin folding also as a consequence of centromere DNA recombination (Giunta and Funabiki, 2017). In our U2OS model, hybridizations of both forward and reverse probes within the same chromatid are depicted (Supplemental Figure 5B, red and green segments) due to inversions and rearrangements of centromere DNA. We also model how the heat denaturation step used in FISH staining may affect the looping organization of DNA of the prometaphase chromosomes by destabilizing the folding and layering of centromere DNA (Supplemental Figure 5C).

The ring-like organization was found in the presence of microtubule depolymerization upon mitotic arrest. Using asynchronous cells without colcemid, even in the absence of microtubule poisons, we still observed a similar ring-like configuration as in arrested metaphase spreads, suggesting that the mitotic architecture of the centromere that we are observing is preserved in the presence or absence of tension derived by microtubule pulling forces. The fact that we also observe ring-like centromeres in anaphase chromosomes (Supplemental Figure 4C) implies that this structural organization of the centromere locus within human chromosomes may be preserved after metaphase throughout mitotic progression and exit. This is also in line with a previous report of a similar rosette-like cluster of CENP-A nucleosomes during the G1 phase of the cell cycle (Andronov, Ouararhni, *et al.*, 2019).

Superresolution microscopy in *Xenopus* egg extracts also detected a ring-like structure upon staining for kinetochore proteins in both *Xenopus* tissue culture cells and human cells (Wynne and Funabiki, 2016). Yet this conformation seems to be transient during the resolution of lateral spindle attachments before the formation of end-on attachments. In the future, it will be important to explore the structural interactions in a 3D space, bringing together data from kinetochore components, the CCAN, centromere chromatin, and the underlying DNA to give a complete picture of the organization at the primary constriction of mitotic chromosomes. Furthermore, future work can integrate chromosome-specific variability and dynamic changes of these structures during chromosome segregation and upon different depolymerizing or microtubule stabilizer drugs. Taking advantage of a gapless human genome (Nurk, Koren, Rhie, Rautiainen, *et al.*, 2022), designing HOR-specific probes will yield additional details of the mitotic human centromere and surrounding DNA. Our work points toward the use of Cen-CO-FISH as an optimal method for superresolution imaging of DNA and prompts more questions on how labeling methods can be further improved to retain a more physiological organization of the DNA, chromatin, and chromosomes (Supplemental Figure 5A) to prevent alteration of the local and higher-order architecture (Supplemental Figure 5C). Altogether, our work adds new information on the ultrastructure of chromosomes to improve our understanding of 3D centromere organization in human mitosis.

MATERIALS AND METHODS

Request a protocol through *Bio-protocol*.

Cell culture

All cells were maintained at 37°C in a 5% CO_2 atmosphere with 21% oxygen. Human immortalized retinal pigmented epithelial RPE-1 cells were grown in DMEM/F-12 media (Life Technologies) supplemented with 10% fetal bovine serum (FBS; Atlanta Biologicals) and 100 U/ml penicillin–streptomycin (P/S; Life Technologies). RPE-1-hTERT cells were obtained from a parental RPE-1 line infected with the pLVX-hTERT-IRES-Hygro lentiviral plasmid and selected for hygromycin resistance and grown in DMEM/F-12, 10% FBS, P/S. U2OS cancer lines were cultured in standard DMEM with 10% FSB and P/S.

CO-FISH

CO-FISH at the centromere was performed as described by Giunta (2018). Briefly, cells were grown in 10 µM BrdU:BrdC (3:1) for 16–18 h before 0.1 µg/ml colcemid (Roche) was added for 2 h. Cells were harvested and swollen in prewarmed 0.075 M KCl at 37°C for 30 min. Cells were then fixed in fresh 3:1 methanol/acetic acid and dropped onto glass slides in a Thermotron Cycler (20°C, 50% humidity) and left in the dark overnight. The slides were rehydrated in 1× phosphate-buffered saline (PBS) for 5 min and treated with RNase A (0.5 µg/ml in PBS; Sigma R5000) for 10 min at 37°C, stained with 0.5 µg/ml Hoechst 33258 (Invitrogen) in 2× saline sodium citrate (SSC) for 10 min at room temperature (RT), and exposed to 365-nm UV light (Stratalinker 1800 UV irradiator) for 30 min. The BrdU/C-labeled DNA strand was digested with 10 U/ml exonuclease III (Promega M1811) for two rounds of 10 min at RT, followed by consecutive incubations with 75, 95, and 100% ethanol. The slides were allowed to air dry overnight before applying hybridizing solution (70% formamide, 1 mg/ml blocking reagent [Roche], 10 mM Tris-HCl, pH 7.2) containing the PNA probe (PNABio) and hybridizing at

RT for 2 h. The slides were washed briefly in wash buffer 1 (70% formamide/10 mM Tris-HCl) before the second 2 h hybridization with the complementary PNA probe (PNABio). Slides were then washed twice in wash buffer 1 for 15 min each wash, followed by three washes in 0.1 M Tris-HCl, pH 7.0/0.15 M NaCl/0.08% Tween-20 (5 min each). DNA was counterstained with (DAPI; Sigma D-9542) added to the second wash. Slides were mounted in antifade reagent (ProLong Glass; Invitrogen) and imaged.

Centromere probes from PNABio were as follows: CENP-B box probe (set 1) against the CENP-B box, F3002 CENP-B Cy3 (ATTC-GTTGGAAACGGGA) and reverse complement CENP-B-RC-488 (TCCCGTTTCCAACGAAT); α-satellite probe against an 18-base-pair consensus sequence within the α-satellite, F3003 CENT-Cy3 (Cy3—OO—AAACTAGACAGAAGCATT) and reverse complement CENT-RC-488 (Alexa-488—O—AATGCTTCTGTCTAGTTT); a second CENP-B box probe (set 2) with inverted fluorophores compared with the other one, F3004 CENP-B-488 (ATTCGTTGGAAACGGGA) and reverse complement CENP-B-RC-Cy3 (TCCCGTTTCCAAC-GAAT) (Giunta and Funabiki, 2017; Giunta, 2018); a table with all sets of probes is given in Supplemental Figure 1B.

FISH

FISH for centromeric DNA was performed as previously described (Giunta, 2018). Briefly, cells were incubated for 2 h with 0.1 µg/ml colcemid. The cells were harvested and fixed as for CO-FISH. After aging overnight, the slides were washed in 1× PBS for 5 min and treated with RNase, followed by consecutive incubation with 75, 95, and 100% ethanol. The slides were allowed to air dry for 30 min before applying a hybridizing solution (70% formamide, 1 mg/ml blocking reagent [Roche], 10 mM Tris-HCl, pH 7.2) containing selected PNA probes (PNABio). The spreads were denatured for 5 min at 80°C on a heat block and hybridized at RT for 2 h. The slides were washed and mounted as for CO-FISH.

Expansion microscopy

The protocol used for ExM was as described previously (Chozinski, Halpern, *et al.*, 2016). RPE-1 cells were enriched for mitotic cells by treatment with 0.1 µg/ml colcemid (Roche) for 2 h. Cells were trypsinized, washed in PBS, and cytospun onto coverslips. The cells were then fixed with 2% PFA (Sigma-Aldrich) and stained with monoclonal CENP-A antibody (Abcam ab13939) and Alexa-488–labeled secondary (Jackson ImmunoResearch 715-547-003). Stained coverslips were then cross-linked with 0.25% glutaraldehyde (Electron Microscopy Sciences 16120) for 10 min. Gelation was then performed with gelation solution (1× PBS, 2 M NaCl, 2.5% [wt/wt] acrylamide, 0.15% [wt/wt] *N,N'*-methylenebisacrylamide, 8.625% [wt/wt] sodium acrylate, 0.2% [wt/wt] ammonium persulfate, and tetramethylethylenediamine) for 30 min. The gelled coverslips were then subjected to protease digestion with 8 U/ml proteinase K (Roche RPROTK-RO) for 60 min at 37°C. Gels were then expanded in 50 ml of deionized water for three 30 min rounds. Gels were cut and imaged on glass-bottomed dishes (MatTek P35G-1.5-14-C) using the 60× silicone oil objective (Olympus UPLSAPO-XS) on a DeltaVision Image Restoration Microscope (GE Healthcare). Sample image z-stacks were deconvolved using SoftWorx (GE Healthcare).

3D SIM

SIM data were acquired using a DeltaVision OMX V4/Blaze 3D SIM superresolution microscope (GE Healthcare) at the Rockefeller University Bio-Imaging Resource Center or an Elyra7 (Zeiss) at the CLN2S-IIT Imaging Facility. The OMX system is fitted with a 100×/1.40 NA UPLSAPO oil objective (Olympus) and three Evolve EMCCD cam-

eras (Photometrics) that were ued in EM gain mode fixed at 170 electrons per count. Immersion oils ranging in refractive index from 1.512 to 1.518 were used depending on the ambient temperature and fluorochromes used. Three laser lines, 405, 488, and 568 nm, were used for excitation, and the corresponding emission filter sets were 436/31, 528/48, and 609/37 nm, respectively. Two identical stacks of optical sections with 125 nm spacing were collected for each data set, first using conventional wide-field illumination of all channels and then using SI of selected channels. The system produces an effective *xy* pixel size of 40 nm in the 3D SIM model. The Elyra7 system with 3D Lattice SIM is equipped with a PlanApo 63×/1.40 NA oil objective (Zeiss) and a cooled sCMOS pco.edge 4.2M camera (PCO; Excelitas Technologies). The system allows the insertion of an additional 1,6× lens, producing an effective pixel size of 62 nm. The laser lines used were 405, 488, and 561 nm. The collected stacks have a 91 nm z-step. The images ware acquired in 3D lattice SIM with a 23 mm grid and 15 phases in frame fast tracks mode.

Image analysis

Following acquisition, the OMX data sets were processed with Soft-WoRx v. 6.1 software (GE Healthcare) using optical transfer functions (OTFs) generated from point spread functions (PSFs) acquired with 100 nm (green and red) or 170 nm (blue) FluoSpheres (Invitrogen/Life Technologies). Wide-field data sets were deconvolved using constrained iterative deconvolution, and SI data sets were reconstructed as described (Schermelleh, Carlton, *et al.*, 2008) using channel-specific k0 values, custom OTFs, and Wiener filters of 0.005, 0.002, and 0.002 for the blue, green, and red channels, respectively. Image registration on the OMX was performed with parameters refined using 100 nm TetraSpeck beads (Invitrogen/Life Technologies). The Elyra7 data set was processed within Zen Black software with the SIM module using the dual iterative SIM (SIM^2) processing and applying an experimental PSF generated from acquisition of 100 nm TetraSpeck beads (Invitrogen/Life Technologies). Imaris software (Bitplane), Metamorph, and ImageJ were used for 3D visualization and generating projection images for visualization and for quantification measurements of individual centromeres from each metaphase spread. ImageJ was used for line scan analysis. Quantification of SI images at centromeres was performed using the Imaris software (Bitplane) surface fitting function and extracting data on each centromere volume and sphericity. All images presented were imported and processed in Photoshop (Adobe Systems).

Quantification of patterned centromeres

To quantify the percentage of patterned centromeres, the maximum-projection images were opened on ImageJ Fiji. The Straight-line tool was selected from the menu to draw a line over the centromeres one by one. From the menu command Analyze was selected the function Plot Profile to show the line scan analysis of the fluorescence intensity. All the graphs were divided into two categories: positive scored and negative scored (different examples are shown in Supplemental Figure 1, D and E); the positive scored are all the centromeres that show a two-peak line scan analysis, and the negative scored show a one-peak plot. For each experiment and each condition, the total number of positive scored centromeres was divided by the total number of chromosomes to calculate the percentage; the data are shown in Figure 2C and Supplemental Figure 2.

REFERENCES

Boldface names denote co–first authors.

Altemose N, Logsdon GA, Bzikadze AV, Sidhwani P, Langley SA, Caldas GV, Hoyt SJ, Uralsky L, Ryabov FD, Shew CJ, *et al.* (2022a). Complete genomic and epigenetic maps of human centromeres. Science 376, eabl4178.

Altemose N, Maslan A, Smith OK, Sundararajan K, Brown RR, Mishra R, Detweiler AM, Neff N, Miga KH, Straight AF, Streets A (2022b). DiMeLo-seq: a long-read, single-molecule method for mapping protein–DNA interactions genome wide. Nat Methods 19, Article 6.

A**ndronov L, Ouararhni K,** Stoll I, Klaholz BP, Hamiche A (2019). CENP-A nucleosome clusters form rosette-like structures around HJURP during G1. Nat Commun 10, Article 1.

Balzano E, Pelliccia F, Giunta S (2021). Genome (in)stability at tandem repeats. Semin Cell Dev Biol 113, 97–112.

Bintu B, Mateo LJ, Su J-H, Sinnott-Armstrong NA, Parker M, Kinrot S, Yamaya K, Boettiger AN, Zhuang X (2018). Super-resolution chromatin tracing reveals domains and cooperative interactions in single cells. Science 362, eaau1783.

Birchler JA, Gao Z, Han F (2009). A tale of two centromeres—diversity of structure but conservation of function in plants and animals. Funct Integr Genomics 9, 7–13.

Black EM, Giunta S (2018). Repetitive fragile sites: centromere satellite DNA as a source of genome instability in human diseases. Genes 9, Article 12.

Blower MD, Sullivan BA, Karpen GH (2002). Conserved organization of centromeric chromatin in flies and humans. Dev Cell 2, 319–330.

Bodor DL, Mata JF, Sergeev M, David AF, Salimian KJ, Panchenko T, Cleveland DW, Black BE, Shah JV, Jansen LE (2014). The quantitative architecture of centromeric chromatin. eLife 3, e02137.

Chardon F, Japaridze A, Witt H, Velikovsky L, Chakraborty C, Wilhelm T, Dumont M, Yang W, Kikuti C, Gangnard S, *et al.* (2022). CENP-B-mediated DNA loops regulate activity and stability of human centromeres. Mol Cell 82, 1751–1767.e8.

Chozinski TJ, Halpern AR, Okawa H, Kim H-J, Tremel GJ, Wong ROL, Vaughan JC (2016). Expansion microscopy with conventional antibodies and fluorescent proteins. Nat Methods 13, Article 6.

Cleveland DW, Mao Y, Sullivan KF (2003). Centromeres and kinetochores: from epigenetics to mitotic checkpoint signaling. Cell 112, 407–421.

Dalal Y, Furuyama T, Vermaak D, Henikoff S (2007). Structure, dynamics, and evolution of centromeric nucleosomes. Proc Natl Acad Sci USA 104, 15974–15981.

Dekker B, Dekker J (2022). Regulation of the mitotic chromosome folding machines. Biochem J 479, 2153–2173.

Gershman A, Sauria MEG, Guitart X, Vollger MR, Hook PW, Hoyt SJ, Jain M, Shumate A, Razaghi R, Koren S, *et al.* (2022). Epigenetic patterns in a complete human genome. Science 376, eabj5089.

Gibcus JH, Samejima K, Goloborodko A, Samejima I, Naumova N, Nuebler J, Kanemaki MT, Xie L, Paulson JR, Earnshaw WC, *et al.* (2018). A pathway for mitotic chromosome formation. Science 359, eaao6135.

Giunta S (2018). Centromere chromosome orientation fluorescent in situ hybridization (Cen-CO-FISH) detects sister chromatid exchange at the centromere in human cells. Bio-Protoc 8, e2792.

Giunta S, Funabiki H (2017). Integrity of the human centromere DNA repeats is protected by CENP-A, CENP-C, and CENP-T. Proc Natl Acad Sci USA 114, 1928–1933.

Giunta S, Hervé S, White RR, Wilhelm T, Dumont M, Scelfo A, Gamba R, Wong CK, Rancati G, Smogorzewska A, *et al.* (2021). CENP-A chromatin prevents replication stress at centromeres to avoid structural aneuploidy. Proc Natl Acad Sci USA 118, e2015634118.

Guenatri M, Bailly D, Maison C, Almouzni G (2004). Mouse centric and pericentric satellite repeats form distinct functional heterochromatin. J Cell Biol 166, 493–505.

Magidson V, Paul R, Yang N, Ault JG, O'Connell CB, Tikhonenko I, McEwen BF, Mogilner A, Khodjakov A (2015). Adaptive changes in the kinetochore architecture facilitate proper spindle assembly. Nat Cell Biol 17, Article 9.

Markaki Y, Smeets D, Cremer M, Schermelleh L (2013). Fluorescence in situ hybridization applications for super-resolution 3D structured illumination microscopy. In: Nanoimaging: Methods and Protocols, ed. AA Sousa, MJ Kruhlak, Humana Press, 43–64.

Marshall OJ, Chueh AC, Wong LH, Choo KHA (2008). Neocentromeres: new insights into centromere structure, disease development, and karyotype evolution. Am J Hum Genet 82, 261–282.

McIntosh JR, Grishchuk EL, West RR (2002). Chromosome-microtubule interactions during mitosis. Annu Rev Cell Dev Biol 18, 193–219.

Nurk S, Koren S, Rhie A, Rautiainen M, Bzikadze AV, Mikheenko A, Vollger MR, Altemose N, Uralsky L, Gershman A, *et al.* (2022). The complete sequence of a human genome. Science 376, 44–53.

Ribeiro SA, Vagnarelli P, Dong Y, Hori T, McEwen BF, Fukagawa T, Flors C, Earnshaw WC (2010). A super-resolution map of the vertebrate kinetochore. Proc Natl Acad Sci USA 107, 10484–10489.

Rieder C, Palazzo R (1992). Colcemid and the mitotic cycle. J Cell Sci 102, 387–392.

Santaguida S, Musacchio A (2009). The life and miracles of kinetochores. EMBO J 28, 2511–2531.

Schalch T, Steiner FA (2017). Structure of centromere chromatin: from nucleosome to chromosomal architecture. Chromosoma 126, 443–455.

Schermelleh L, Carlton PM, Haase S, Shao L, Winoto L, Kner P, Burke B, Cardoso MC, Agard DA, Gustafsson MGL, *et al.* (2008). Subdiffraction multicolor imaging of the nuclear periphery with 3D structured illumination microscopy. Science 320, 1332–1336.

Schermelleh L, Heintzmann R, Leonhardt H (2010). A guide to super-resolution fluorescence microscopy. J Cell Biol 190, 165–175.

Su J-H, Zheng P, Kinrot SS, Bintu B, Zhuang X (2020). Genome-scale imaging of the 3D organization and transcriptional activity of chromatin. Cell 182, 1641–1659.e26.

Sullivan BA (2010). Optical mapping of protein–DNA complexes on chromatin fibers. In: Fluorescence In Situ Hybridization (FISH): Protocols and Applications, ed. JM Bridger, EV Volpi, Humana Press, 99–115.

Sullivan BA, Karpen GH (2004). Centromeric chromatin exhibits a histone modification pattern that is distinct from both euchromatin and heterochromatin. Nat Struct Mol Biol 11, Article 11.

Sullivan LL, Boivin CD, Mravinac B, Song IY, Sullivan BA (2011). Genomic size of CENP-A domain is proportional to total alpha satellite array size at human centromeres and expands in cancer cells. Chromosome Res 19, 457.

Vagnarelli P, Earnshaw WC (2001). INCENP loss from an inactive centromere correlates with the loss of sister chromatid cohesion. Chromosoma 110, 393–401.

Vagnarelli P, Ribeiro SA, Earnshaw WC (2008). Centromeres: old tales and new tools. FEBS Lett 582, 1950–1959.

Verdaasdonk JS, Bloom K (2011). Centromeres: unique chromatin structures that drive chromosome segregation. Nat Rev Mol Cell Biol 12, Article 5.

Walstein K, Petrovic A, Pan D, Hagemeier B, Vogt D, Vetter IR, Musacchio A (2021). Assembly principles and stoichiometry of a complete human kinetochore module. Sci Adv 7, eabg1037.

Winkler R, Perner B, Rapp A, Durm M, Cremer C, Greulich K-O, Hausmann M (2003). Labelling quality and chromosome morphology after low temperature FISH analysed by scanning far-field and near-field optical microscopy. J Microsc 209, 23–33.

Wynne DJ, Funabiki H (2016). Heterogeneous architecture of vertebrate kinetochores revealed by three-dimensional superresolution fluorescence microscopy. Mol Biol Cell 27, 3395–3404.

Yeh E, Haase J, Paliulis LV, Joglekar A, Bond L, Bouck D, Salmon ED, Bloom KS (2008). Pericentric chromatin is organized into an intramolecular loop in mitosis. Curr Biol 18, 81–90.

Zinkowski RP, Meyne J, Brinkley BR (1991). The centromere-kinetochore complex: a repeat subunit model. J Cell Biol 113, 1091–1110.